Noise Bounds in Multicarrier mmWave Doppler Measurements

Martin Lerch*†, Erich Zöchmann†, Sebastian Caban*†, and Markus Rupp†
*Christian Doppler Laboratory for Dependable Wireless Connectivity for the Society in Motion
†Institute of Telecommunications, TU Wien, Austria
mlerch@nt.tuwien.ac.at

***Abstract*—More and more research groups are working on experimental research of millimeter wave (mmWave) wireless communications. Up to now, most mmWave measurements have been carried out in static scenarios. However, as the Doppler effect scales linearly with the carrier frequency, mmWave multicarrier transmission is prone to intercarrier interference caused by Doppler shifts. Today, mmWave radio frequency chipsets (mostly designed for IEEE 802.11ad) are not of as high quality as their centimeter-wave counterparts. Especially the phase noise performance and the noise figure are much worse. Using a testbed with off-the-shelf transmit and receive modules, we show that, depending on the subcarrier spacing, thermal noise or phase noise is dominating the effects of Doppler shifts. Thus, care must be taken in the designing phase of mmWave Doppler measurements.**

I. Introduction

To meet the peak data rate demands of next generations mobile communications, researchers propose to unlock the underutilized spectrum in the millimeter wave (mmWave) bands [1], [2]. In order to investigate the channel characteristics in these frequency bands and, in the next step, to evaluate the performance of different transmission modes [3], experimental research relys on dedicated measurement equipment and testbeds. For channel sounding type of measurements the sounding equipment can either be a vector network analyzer [4]–[6] or can be based on correlative or UWB channel sounders [7]–[9]. Performance measurements require more flexible setups that allow for experiments with arbitrary signals. Thereby, existing general purpose testbeds are mainly based on commercial baseband devices and external mixers to enable a Software Defined Radio (SDR) approach [10]–[13]. Fewer research groups use measurement grade equipment such as arbitrary waveform transmitters [14], [15] and high sample rate receivers such as ADC cards or digital storage oscilloscopes. The latter approach allows for time and frequency synchronization in hardware [16], so that the performance of frequency offset compensation algorithms and frame start detection algorithms do not impact the results obtained.

Experiments at high velocities

Now that the first measurement setups are available, some research groups are pushing forward to high mobility scenarios (see [17]–[21] for channel sounding concepts and experimental setups and [22] for a general overview). Especially for upcoming mmWave vehicular communications [23], measurements involving fast-fading channels will be present. Thereby, on the one hand, time-variant channels cause channel interpolation errors [24], [25], and on the other hand, when using multicarrier modulation schemes like Orthogonal Frequency Division Multiplexing (OFDM) or Filter Bank Multi-Carrier modulation [26], [27] Doppler shifts cause Inter-Carrier-Interference (ICI). Thereby, the extent of ICI increases with velocity and carrier frequency and decreases with subcarrier spacing [28]–[30]. Thus, the subcarrier spacing is an important design parameter of wireless communication systems for high mobility scenarios. Therefore, measurement setups for experiments focusing on the impact of Doppler need to be designed such that the ICI due to Doppler shifts dominates all other sources of interference within the range of subcarrier spacings and within the range of velocities under investigation.

Our Contribution

We show — based on our own mmWave testbed — that for different subcarrier spacings, interference is dominated by different noise sources. Doppler effects are only observable, if the strength of the Doppler interference is above thermal noise, phase noise, and quantization noise.

II. Our mmWave Testbed

The mmWave testbed in this work implements an SDR approach [31], [32] that allows for transmissions of arbitrary signals over a 60 GHz wireless link. Thereby, the transmit signals are first pre-generated off-line and then transmitted blockwise signal-by-signal over the wireless link. The received signals are recorded for later off-line evaluation.

Figure 1 illustrates the testbed, that is built around an off-the-shelf 60 GHz link consisting of a pair of a transmit module and a receive module [33] allowing for transmissions of arbitrary I/Q baseband signals with bandwidths of up to 1.8 GHz. The carrier frequency can be set in steps of approximately 500 MHz within the range of 57 GHz to 64 GHz. At the transmitter side, the I/Q baseband signals provided to the transmitter module are generated by an Arbitrary Waveform Generator (AWG) that plays back pre-generated waveforms over up to four independent DAC channels with a sample rate of 16 GSa/s. At the receiver side, the received I/Q baseband signals are sampled by an ADC board, capable of recording up to four baseband signals with a sampling rate of 200 MSa/s. The received samples are directly saved to a hard disk drive.

ISBN 978-3-8007-4426-8

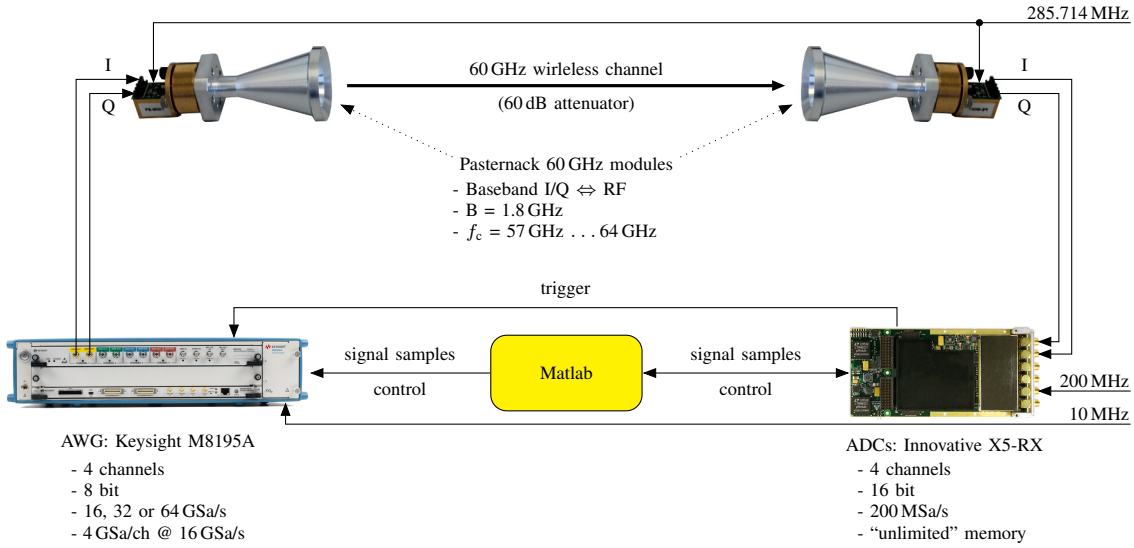

Fig. 1. Setup and main parameters of the mmWave testbed built around an off-the-shelf 60 GHz link.

This approach allows to record signals in nearly real-time. The maximum length of a single transmit signal is limited by the AWG in the transmitter to 250 ms. The useable bandwidth is limited by the sampling rate of the receiver ADCs to less than 200 MHz.

In this paper, we only consider perfectly synchronized back-to-back measurements via a 60 dB attenuator to exclude the effects of a time-varying channel [34] and focus on the performance of our hardware. To avoid nonlinearities, transmitter and receiver are only operated in their linear range.

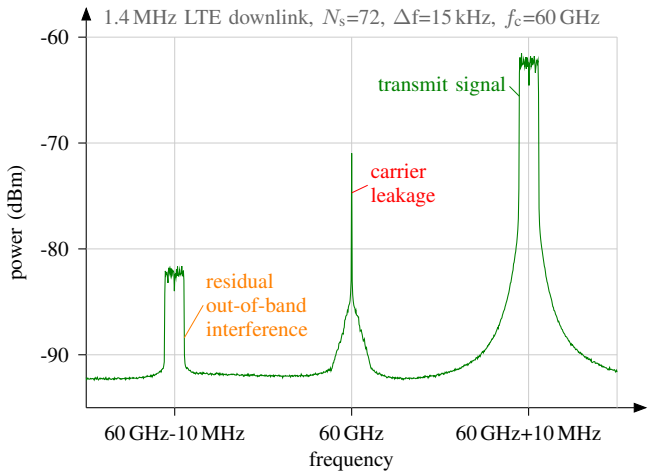

Fig. 2. Spectrum of the multicarrier signal transmitted at 60 GHz. Interference due to I/Q imbalance and carrier leakage is avoided by digital upconversion.

Interference due to I/Q imbalance and carrier leakage is avoided by digital upconversion in the AWG. Thereby, we transmit the Intermediate Frequency signal in the in-phase (I) and its Hilbert transform in the quadrature-phase (Q). After up-conversion, the resulting transmit signal at 60 GHz thus contains, next to the leaked carrier and the transmit signal, also a signal image in the lower sideband (see Figure 2). In-band reception of this residual out-of-band interference due to transmitter I/Q imbalance is then avoided in the receiver by using a local oscillator (LO) frequency different from the LO frequency used in the transmitter. Consequently, after reception, the in-phase and the Hilbert transformed quadrature signals are added to reconstruct the transmitted signal without losing Signal-to-Noise Ratio (SNR).

III. Thermal Noise

In this work we compare OFDM signals with different subcarrier spacings. We consider a constant total transmit power P_{TX} and a constant number of subcarriers N_{s} and therefore a constant transmit power per subcarrier $\frac{P_{\mathrm{TX}}}{N_{\mathrm{s}}}$. Furthermore, the per-subcarrier power after the Fast Fourier Transform (FFT) is independent of the subcarrier spacing $\Delta\mathrm{f}$ when considering a fixed sampling rate f_s and a $1/N_{\mathrm{FFT}} = \frac{\Delta\mathrm{f}}{f_s}$ scaling in the FFT of the received samples $y\,[n]$:

$$Y\,[k] = \frac{1}{N_{\mathrm{FFT}}} \sum_{n=0}^{N_{\mathrm{FFT}}-1} e^{-j2\pi \frac{kn}{N_{\mathrm{FFT}}}} \cdot y\,[n]\,. \tag{1}$$

Using this scaling, the post-FFT noise power is not independent of the subcarrier spacing. Considering additive white noise with a power spectral density N_0, the total noise power within the receiver bandwidth B_{RX}=$N_{\mathrm{FFT}}\Delta\mathrm{f}$ calculates to σ_{n}^2=$N_0 B_{\mathrm{RX}}$. The per-subcarrier noise power after the FFT is then given by

$$\sigma_{\mathrm{n,sc}}^2 = \frac{\sigma_{\mathrm{n}}^2}{N_{\mathrm{FFT}}} = \frac{\sigma_{\mathrm{n}}^2}{B_{\mathrm{RX}}}\Delta\mathrm{f} = N_0\Delta\mathrm{f} \tag{2}$$

and scales linearly with the subcarrier spacing $\Delta\mathrm{f}$.

IV. Quantization Noise

Quantization noise limits the achievable Signal-to-Interference Ratio (SIR) at the transmitter and at the receiver.

ISBN 978-3-8007-4426-8

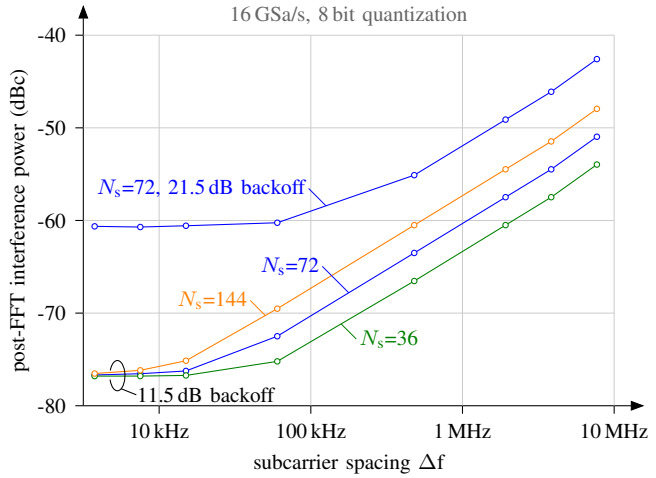

Fig. 3. Impact of quantization noise on OFDM transmissions. The interference increases with subcarrier spacing and the number of subcarriers.

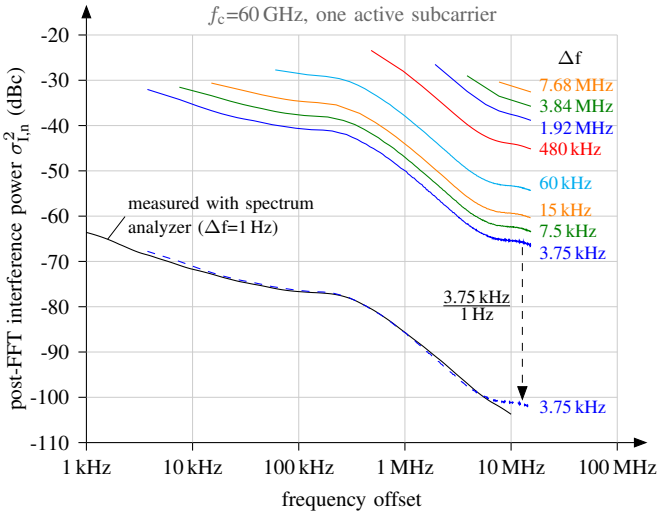

Fig. 4. Phase noise characteristic of our mmWave testbed obtained through FFT analysis and by a spectrum analyzer. The interference due to phase noise increases with increasing subcarrier spacing.

We use 8-bit DACs at the transmitter and 16-bit quantization at the receiver. At our testbed receiver, no automatic gain control is applied; thereby the impact of quantization noise is receive power dependent. Still, the transmitter is our quantization noise limiting device.

Peak-to-Average Power Ratio

The SIR due to quantization noise generated in the transmitter furthermore depends on the Peak-to-Average Power Ratio (PAPR) of the transmit signals and the input-backoff [35] used. Thereby, depending on the PAPR, the input-backoff trades off between clipping and quantization noise. For passband OFDM signals, the upper bound of the PAPR is given by the worst case when all N_s subcarriers are being modulated with the same data symbol:

$$\mathrm{PAPR}_{\max} = 3.01\,\mathrm{dB} + 10 \cdot \log_{10}(N_s)\,\mathrm{dB}. \quad (3)$$

Thereby, the PAPR depends on the number of subcarriers but is independent of the subcarrier spacing [36]. For N_s=72 subcarriers, the maximum PAPR is approximately 21.5 dB. In Figure 3, the interference due to quantization is shown for two different values of input-backoff. The maximum quantization noise is obtained when clipping is completely avoided by using a backoff that equals the maximum PAPR of 21.5 dB. Allowing for clipping by down-scaling the transmit signals before the quantization to obtain an input backoff of 11.5 dB (as in [35]) yields a higher number of effective bits. The impact of quantization noise on OFDM transmissions increases with subcarrier spacing and the number of subcarriers.

V. Phase Noise

Phase noise affects OFDM transmissions in two ways. On the one hand, every subcarrier generates ICI onto other subcarriers. On the other hand, all subcarriers within one OFDM symbol experience exactly the same common phase error (CPE) that varies only over OFDM symbol time-index. Thereby, the impact of the CPE on OFDM transmissions depends on the pattern of the reference symbols used for channel estimation [37]. Considering reference symbols in every OFDM symbol, the impact of the CPE can be completely eliminated while the actual channel estimates are still disturbed by ICI. Therefore, we limit the analysis of phase noise as limiting factor on OFDM transmissions on the effect of ICI. Thereby, we analyze the effect of phase noise induced by the mmWave testbed on OFDM transmissions step-by-step. We measured the phase noise characteristic by transmitting a single carrier before we estimate the ICI-power for OFDM transmissions by summation. Directly measuring the phase noise performance was not possible for subcarrier spacings larger than 1 MHz due to bandwidth and SNR limitations in our testbed.

Phase noise characteristic

In order to measure the phase noise characteristic of the mmWave testbed, we transmit a sine-wave at 60 GHz and evaluate the response of the testbed at the output of the receiver module. The thereby measured phase noise characteristic comprises phase noise contributions by the AWG, the reference oscillator, both 60 GHz modules and the receiver ADCs. The results in terms of post-FFT power below carrier are shown in Figure 4 where we compare the results obtained through FFT analysis using different FFT-lengths to the result of a phase noise measurement performed with a spectrum analyzer[1]. Thereby, the result obtained with the spectrum analyzer corresponds to an FFT-measurement using a subcarrier spacing (resolution bandwidth) of 1 Hz. The results $\sigma^2_{I,n}$ obtained through FFT analysis illustrate the effect of phase noise on OFDM signals with different subcarrier spacings. Even though the phase noise decreases with increasing frequency, the interference power after the FFT increases with increasing

[1]Rohde & Schwarz FSW-50

ISBN 978-3-8007-4426-8

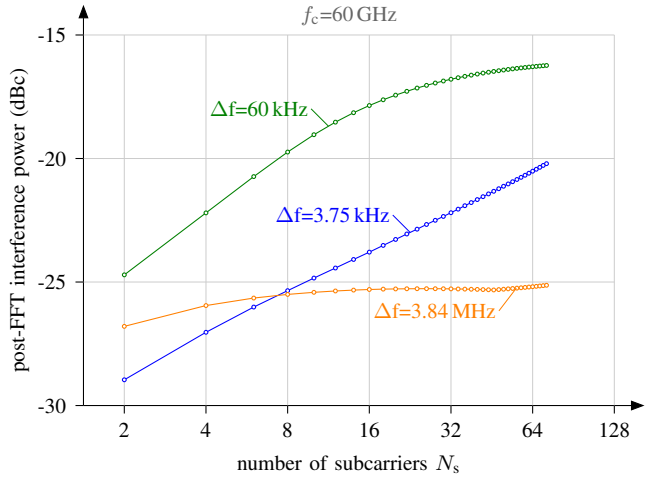

Fig. 5. ICI due to phase noise for different numbers of subcarriers. The higher the subcarrier spacing the less subcarriers contribute to the total ICI.

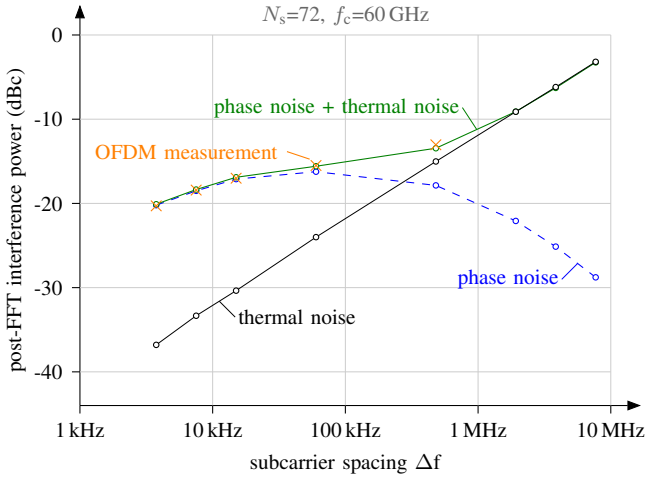

Fig. 6. ICI due to phase noise for different subcarrier spacings. For small subcarrier spacings interference due to phase noise dominates the receiver noise while for large subcarrier spacings, receiver noise dominates.

subcarrier spacing. Thereby, a higher subcarrier spacing corresponds to a higher noise bandwidth. As long as the decay of the phase noise characteristic is below 10 dB/decade, the interference generated on the next subcarrier increases with increasing subcarrier spacing. For subcarrier spacings larger than 480 kHz, the interference on the next subcarrier decreases with increasing subcarrier spacing.

ICI due to phase noise

For the evaluation of the total interference power when transmitting an OFDM signal with a certain number of subcarriers we use the afore obtained results $\sigma^2_{\mathrm{I,n}}$ and sum up the interference from all subcarriers N_s involved. Thereby we consider uncorrelated subcarriers and consider the worst case by evaluating the interference on the central subcarrier:

$$\sigma^2_{\mathrm{ICI}} = 2 \sum_{n=1}^{N_s/2} \sigma^2_{\mathrm{I,n}}. \tag{4}$$

The results for different numbers of subcarriers are shown in Figure 5. Thereby, the number of subcarriers contributing to the total ICI-power depends on the subcarrier spacing. The higher the subcarrier spacing, the less subcarriers contribute to the ICI-power and a saturation of the ICI-power is observed. In the results shown in Figure 6 we fix the number of subcarriers to N_s=72 and, in addition, consider the impact of white noise (see (2)). While the ICI-power due to phase noise reaches a maximum for a subcarrier spacing of approx. 60 kHz, the impact of white noise increases with increasing subcarrier spacing. Thereby, we observe a break-even point where the impact of noise becomes stronger than the ICI due to phase noise. Its position in terms of subcarrier spacing depends on the value of the input backoff introduced in Section IV. In order to cross-check the results obtained by summing up interference, we compare them to the estimated Interference-plus-Noise power when actually transmitting an OFDM signal with N_s=72 subcarriers.

VI. ICI due to Doppler

For the well known Jakes' Doppler spectrum the ICI can be analytically evaluated [28]. Due to the lack of measurements we evaluate this analytical expression at a carrier frequency of 60 GHz, various velocities, and various subcarrier spacings.

VII. Discussion and Conclusion

Figure 7 shows the noise and interference sources within our testbed:

(1) Thermal Noise: While the power spectral density of the thermal noise is fixed, its impact on OFDM transmissions increases with subcarrier spacing for a constant number of subcarriers. Being limited by thermal noise can be treated by increasing the received signal power by an additional power amplifier in the transmitter.

(2) Phase Noise: The impact of phase noise depends on the subcarrier spacing and the number of subcarriers used. Unlike thermal noise, it scales with the actual signal power in the transmitter and the receiver. A system limited by phase noise can not be improved by amplifying the transmit signal. Better, very costly, oscillators are needed.

(3) Quantization Noise: The impact of quantization noise increases with increasing subcarrier spacing and increasing number of subcarriers. In our setup, the contribution of quantization noise to the overall interference is negligible. Remember, our 8-bit DAC has an oversampling factor of greater 80 and our ADC comes with 16-bit resolution. However, in other setups, quantization noise may matter.

(4) ICI due to Doppler: Assuming a Jakes' Doppler spectrum, the intercarrier interference is shown in Figure 7. As lower border, we illustrate a pedestrian speed of 6 km/h. As upper border, we choose the extreme example of 500 km/h. Even at that speed, for subcarrier spacings larger than 150 kHz, the ICI is buried in noise.

ISBN 978-3-8007-4426-8

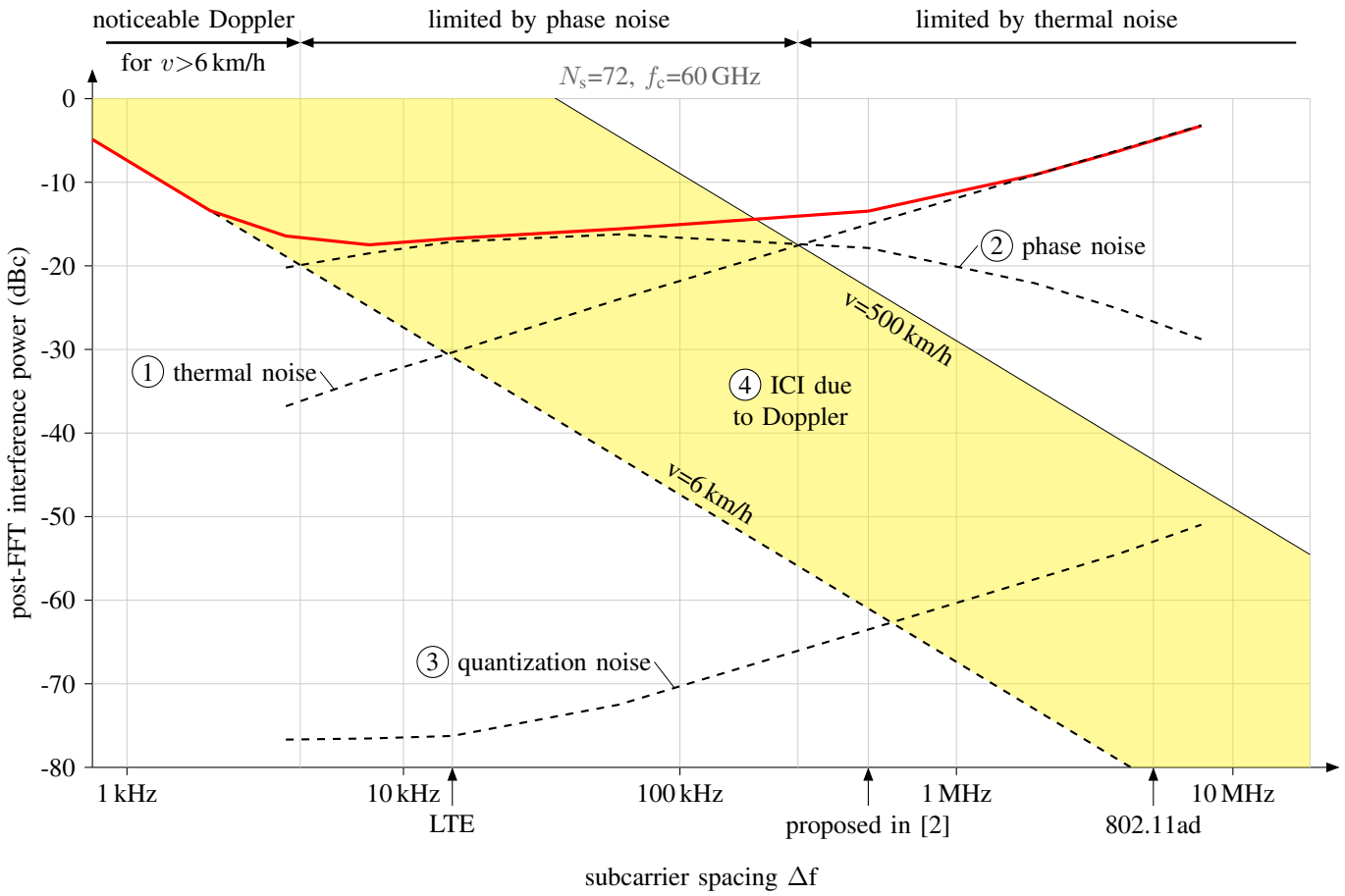

Fig. 7. Noise bounds in multicarrier mmWave Doppler measurements using the example of our specific testbed. For small subcarrier spacings, ICI due to Doppler is noticeable, while for larger subcarrier spacings, phase noise and then receiver noise dominates. The impact of quantization noise is negligible.

We therefore conclude for different wireless communication standards:

- *LTE @ 60 GHz*: With a subcarrier spacing of 15 kHz, "LTE like" signals are prone to ICI due to Doppler. In our specific setup, LTE signals [38], [39] are in the phase noise limited regime. A post-FFT Signal-to-Interference-plus-Noise Ratio (SINR) will never be larger than 18 dB.
- *5G mmWave*: The work of [2] has proposed to use a subcarrier spacing of 480 kHz for mmWave broadband systems. That proposal is limited by thermal and phase noise within our testbed built with representative off-the-shelf components. As above, the SINR will not be greater than 18 dB due to phase noise.
- *IEEE 802.11ad*: The 60 GHz WLAN standard proposes a subcarrier spacing of 5.15625 MHz. For this choice, the testbed is in the thermal noise limited regime. As mentioned above, the SINR can costly be improved by a power amplifier at the transmitter. In testbeds with worse DACs or ADCs, quantization noise could be already almost as strong as phase noise.

Thus, not only thermal noise, but also phase noise and quantization noise must be taken into account when choosing the subcarrier spacing in mmWave communications. In our setup, ICI due to Doppler shifts is only observable, if the subcarrier spacing is low enough.

On the contrary, when comparing measurements with theory which only considers thermal noise, measurements need to be performed in a region where thermal noise dominates all other sources of interference. In previous measurements [40] that were performed with the same testbed, we used a subcarrier spacing of 500 kHz. Thereby, due to phase noise, a deviation from theory was already visible for moderate values of SNR.

Acknowledgments

This work has been funded by A1 Telekom Austria AG and the Institute of Telecommunications, TU Wien. The financial support by the Austrian Federal Ministry of Science, Research and Economy and the National Foundation for Research, Technology and Development is gratefully acknowledged. The research has been co-financed by the Czech Science Foundation, Project No. 17-18675S "Future transceiver techniques for the society in motion" and by the Czech Ministry of Education in the frame of the National Sustainability Program under grant LO1401.

REFERENCES

[1] E. Dahlman, G. Mildh, S. Parkvall, J. Peisa, J. Sachs, Y. Selén, and J. Sköld, "5G wireless access: requirements and realization," *IEEE Communications Magazine*, vol. 52, no. 12, pp. 42–47, 2014.

[2] Z. Pi and F. Khan, "An introduction to millimeter-wave mobile broadband systems," *IEEE Communications Magazine*, vol. 49, no. 6, 2011.

[3] M. Lerch and M. Rupp, "Measurement-Based Evaluation of the LTE MIMO Downlink at Different Antenna Configurations," in *Proc. of the 17th International ITG Workshop on Smart Antennas 2013 (WSA 2013)*, Stuttgart, Germany, Feb. 2013.

[4] C. Gustafson, K. Haneda, S. Wyne, and F. Tufvesson, "On mm-wave multipath clustering and channel modeling," *IEEE Transactions on Antennas and Propagation*, vol. 62, no. 3, pp. 1445–1455, 2014.

[5] J. Blumenstein, T. Mikulasek, T. Zemen, C. Mecklenbräuker, R. Marsalek, and A. Prokes, "In-vehicle mm-wave channel model and measurement," in *Proc. of IEEE Vehicular Technology Conference (VTC Fall)*, 2014, pp. 1–5.

[6] E. Zöchmann, M. Lerch, S. Caban, R. Langwieser, C. F. Mecklenbräuker, and M. Rupp, "Directional evaluation of receive power, Rician K-factor and RMS delay spread obtained from power measurements of 60GHz indoor channels," in *IEEE-APS Topical Conference on Antennas and Propagation in Wireless Communications (APWC 2016)*, Cairns, Australia, Sep. 2016.

[7] T. S. Rappaport, S. Sun, R. Mayzus, H. Zhao, Y. Azar, K. Wang, G. N. Wong, J. K. Schulz, M. Samimi, and F. Gutierrez, "Millimeter wave mobile communications for 5G cellular: It will work!" *IEEE Access*, vol. 1, pp. 335–349, 2013.

[8] S. Häfner, D. A. Dupleich, R. Müller, J. Luo, E. Schulz, C. Schneider, R. S. Thomä, X. Lu, and T. Wang, "Characterisation of channel measurements at 70 GHz in indoor femtocells," in *81st IEEE Vehicular Technology Conference (VTC Spring)*, 2015, pp. 1–5.

[9] T. Zwick, T. J. Beukema, and H. Nam, "Wideband channel sounder with measurements and model for the 60 GHz indoor radio channel," *IEEE Transactions on Vehicular Technology*, vol. 54, no. 4, pp. 1266–1277, 2005.

[10] W. Keusgen, A. Kortke, M. Peter, and R. Weiler, "A highly flexible digital radio testbed and 60 GHz application examples," in *Proc. of IEEE European Microwave Conference (EuMC)*, 2013, pp. 740–743.

[11] J. Arnold, L. Simic, M. Petrova, and P. Mähönen, "Demo: Spectrum-agile mm-wave packet radio implementation on USRPs," in *Proc. of the Workshop on Software Radio Implementation Forum*. ACM, 2015, pp. 5–8.

[12] J. Zhang, X. Zhang, P. Kulkarni, and P. Ramanathan, "OpenMili: a 60 GHz software radio platform with a reconfigurable phased-array antenna," in *Proc. of the Annual International Conference on Mobile Computing and Networking*. ACM, 2016, pp. 162–175.

[13] P. Zetterberg and R. Fardi, "Open source SDR frontend and measurements for 60-GHz wireless experimentation," *IEEE Access*, vol. 3, pp. 445–456, 2015.

[14] N. Preyss, R. D. Pantić, and A. Burg, "Correlation based phase noise compensation in 60 GHz wireless systems," in *Proc. of IEEE Convention of Electrical & Electronics Engineers in Israel (IEEEI)*, 2014, pp. 1–5.

[15] N. Preyss, L. Koestler, and A. Burg, "Fractionally spaced complex sub-nyquist sampling for multi-gigabit 60 GHz wireless communication," in *Proc. of IEEE International Midwest Symposium on Circuits and Systems (MWSCAS)*, 2015, pp. 1–4.

[16] S. Caban, A. Disslbacher-Fink, J. A. García Naya, and M. Rupp, "Synchronization of wireless radio testbed measurements," in *Proc. IEEE International Instrumentation and Measurement Technology Conference (I2MTC2011)*, 2011.

[17] E. Zöchmann, S. Caban, M. Lerch, and M. Rupp, "Resolving the angular profile of 60 GHz wireless channels by Delay-Doppler measurements," in *IEEE 9th Sensor Array and Multichannel Signal Processing Workshop (SAM 2016)*, Rio de Janeiro, Brazil, Jul. 2016.

[18] P. B. Papazian, C. Gentile, K. A. Remley, J. Senic, and N. Golmie, "A radio channel sounder for mobile millimeter-wave communications: System implementation and measurement assessment," *IEEE Transactions on Microwave Theory and Techniques*, vol. 64, no. 9, pp. 2924–2932, 2016.

[19] E. Zöchmann, R. Langwieser, S. Caban, M. Lerch, S. Pratschner, R. Nissel, C. Mecklenbräuker, and M. Rupp, "A millimeter wave testbed for repeatable high velocity measurements," in *European Wireless 2017 (EW2017)*, Dresden, Germany, May 2017.

[20] S. Caban, J. Rodas, and J. A. García-Naya, "A Methodology for Repeatable, Off-line, Closed-loop Wireless Communication System Measurements at Very High Velocities of up to 560 km/h," in *Proc. International Instrumentation and Measurement Technology Conference (I2MTC 2011)*, Binjiang, Hangzhou, China, May 2011.

[21] R. Nissel, M. Lerch, and M. Rupp, "Experimental validation of the OFDM bit error probability for a moving RX antenna," in *IEEE Vehicular Technology Conference (VTC)*, Vancouver, Canada, Sep. 2014.

[22] S. Schwarz and M. Rupp, "Society in motion: Challenges for LTE and beyond mobile communications," *IEEE Communications Magazine*, vol. 54, no. 5, pp. 76–83, 2016.

[23] V. Va, T. Shimizu, G. Bansal, and R. W. Heath Jr, "Millimeter wave vehicular communications: A survey," *Foundations and Trends® in Networking*, vol. 10, no. 1, pp. 1–113, 2016.

[24] M. Lerch, "Experimental comparison of fast-fading channel interpolation methods for the LTE uplink," in *Proc. of the 57th International Symposium ELMAR-2015*, Zadar, Croatia, Sep. 2015.

[25] R. Nissel, M. Lerch, M. Simko, and M. Rupp, "Bit error probability for pilot-symbol-aided OFDM channel estimation in doubly-selective channels," in *International ITG Workshop on Smart Antennas (WSA)*, Erlangen, Germany, Feb. 2014.

[26] R. Nissel and M. Rupp, "Enabling low-complexity MIMO in FBMC-OQAM," in *IEEE Globecom Workshops (GC Wkshps)*, Washington, USA, Dec. 2016.

[27] J. Rodríguez-Piñeiro, M. Lerch, T. Domínguez-Bolaño, J. A. García-Naya, S. Caban, and L. Castedo, "Experimental assessment of 5G-Candidate modulation schemes at extreme speeds," in *IEEE 9th Sensor Array and Multichannel Signal Processing Workshop (SAM 2016)*, Rio de Janeiro, Brazil, Jul. 2016.

[28] P. Robertson and S. Kaiser, "The effects of Doppler spreads in OFDM (A) mobile radio systems," in *IEEE Vehicular Technology Conference, Fall*, vol. 1. IEEE, 1999, pp. 329–333.

[29] J. Rodríguez-Piñeiro, M. Lerch, P. Suárez-Casal, J. A. García-Naya, S. Caban, M. Rupp, and L. Castedo, "LTE Downlink Performance in High Speed Trains," in *Proceedings of the 81st Vehicular Technology Conference (VTC2015-Spring)*, Glasgow, Scotland, May 2015.

[30] J. Rodríguez-Piñeiro, M. Lerch, J. A. García-Naya, S. Caban, M. Rupp, and L. Castedo, "Emulating Extreme Velocities of Mobile LTE Receivers in the Downlink," *special issue JWCN*, 2015.

[31] M. Lerch, S. Caban, M. Mayer, and M. Rupp, "The Vienna MIMO testbed: Evaluation of future mobile communication techniques," *Intel Technology Journal*, vol. 18, pp. 58–69, 2014.

[32] C. Mehlführer, S. Geirhofer, S. Caban, and M. Rupp, "A flexible MIMO testbed with remote access," in *Proc. of the 13th European Signal Processing Conference (EUSIPCO 2005)*, Antalya, Turkey, Sep. 2005.

[33] 60 GHz transmitter and 60 GHz receiver module. (Date last accessed 14-02-2017). [Online]: https://www.pasternack.com/60-ghz-modules-category.aspx

[34] M. Lerch, S. Caban, E. Zöchmann, and M. Rupp, "Quantifying the repeatability of wireless channels by quantized channel state information," in *IEEE 9th Sensor Array and Multichannel Signal Processing Workshop (SAM 2016)*, Rio de Janeiro, Brazil, Jul. 2016.

[35] T. Jiang and Y. Wu, "An overview: Peak-to-average power ratio reduction techniques for OFDM signals," *IEEE Transactions on Broadcasting*, vol. 54, no. 2, pp. 257–268, June 2008.

[36] M. Lerch, J. Rodríguez-Piñeiro, J. A. García-Naya, and L. Castedo, "Methods to perform high velocity LTE experiments at low velocities," in *IEEE 83rd Vehicular Technology Conference (VTC2016-Spring)*, Nanjing, China, May 2016.

[37] P. Robertson and S. Kaiser, "Analysis of the effects of phase-noise in orthogonal frequency division multiplex (OFDM) systems," in *IEEE International Conference on Communications (ICC)*, vol. 3, Jun. 1995, pp. 1652–1657 vol.3.

[38] M. Rupp, S. Schwarz, and M. Taranetz, *The Vienna LTE-Advanced Simulators: Up and Downlink, Link and System Level Simulation*, 1st ed., ser. Signals and Communication Technology. Springer Singapore, 2016.

[39] E. Zöchmann, S. Schwarz, S. Pratschner, L. Nagel, M. Lerch, and M. Rupp, "Exploring the physical layer frontiers of cellular uplink," *EURASIP Journal on Wireless Communications and Networking*, vol. 2016, no. 1, pp. 1–18, 2016.

[40] R. Nissel, E. Zöchmann, M. Lerch, S. Caban, and M. Rupp, "Low-latency MISO FBMC-OQAM: It works for millimeter waves!" in *IEEE International Microwave Symposium (IMS)*, Hawaii, USA, Jun. 2017.

ISBN 978-3-8007-4426-8